2-16-2017

Cosmogenic $^{26}Al/^{10}Be$ surface production ratio in Greenland

Lee B. Corbett
University of Vermont

Paul R. Bierman
University of Vermont

Dylan H. Rood
Imperial College London

Marc W. Caffee
College of Science

Nathaniel A. Lifton
College of Science

See next page for additional authors

Recommended Citation

Corbett, L. B., Bierman, P. R., Rood, D. H., Caffee, M. W., Lifton, N. A., and Woodruff, T. E. (2017), Cosmogenic 26Al/10Be surface production ratio in Greenland, Geophys. Res. Lett., 44, 1350– 1359, doi:10.1002/2016GL071276.

AGU PUBLICATIONS

Geophysical Research Letters

RESEARCH LETTER
10.1002/2016GL071276

Key Points:
- The cosmogenic $^{26}Al/^{10}Be$ production ratio in quartz is higher than traditionally thought and likely varies with latitude/altitude
- Using continually exposed rock surfaces in Greenland, we constrain the high-latitude $^{26}Al/^{10}Be$ production ratio to 7.3 ± 0.3
- A higher assumed $^{26}Al/^{10}Be$ production ratio results in greater modeled burial durations and erosion rates

Supporting Information:
- Supporting Information S1

Correspondence to:
L. B. Corbett,
Ashley.Corbett@uvm.edu

Citation:
Corbett, L. B., P. R. Bierman, D. H. Rood, M. W. Caffee, N. A. Lifton, and T. E. Woodruff (2017), Cosmogenic $^{26}Al/^{10}Be$ surface production ratio in Greenland, *Geophys. Res. Lett.*, *44*, 1350–1359, doi:10.1002/2016GL071276.

Received 20 SEP 2016
Accepted 12 JAN 2017
Accepted article online 15 JAN 2017
Published online 2 FEB 2017

Cosmogenic $^{26}Al/^{10}Be$ surface production ratio in Greenland

Lee B. Corbett[1], Paul R. Bierman[1], Dylan H. Rood[2], Marc W. Caffee[3,4], Nathaniel A. Lifton[4,3], and Thomas E. Woodruff[3]

[1]Department of Geology, University of Vermont, Burlington, Vermont, USA, [2]Department of Earth Science and Engineering, Imperial College London, London, UK, [3]Department of Physics and Astronomy, Purdue University, West Lafayette, Indiana, USA, [4]Department of Earth, Atmospheric, and Planetary Sciences, Purdue University, West Lafayette, Indiana, USA

Abstract The assumed value for the cosmogenic $^{26}Al/^{10}Be$ surface production rate ratio in quartz is an important parameter for studies investigating the burial or subaerial erosion of long-lived surfaces and sediments. Recent models and data suggest that the production ratio is spatially variable and may be greater than originally thought. Here we present measured $^{26}Al/^{10}Be$ ratios for 24 continuously exposed bedrock and boulder surfaces spanning ~61–77°N in Greenland. Empirical measurements, such as ours, include nuclides produced predominately by neutron-induced spallation with percent-level contributions by muon interactions. The slope of a York regression line fit to our data is 7.3 ± 0.3 (1σ), suggesting that the $^{26}Al/^{10}Be$ surface production ratio exceeds the commonly used value of 6.75, at least in the Arctic. A higher $^{26}Al/^{10}Be$ production ratio has implications for multinuclide cosmogenic isotope studies because it results in greater modeled burial durations and erosion rates.

1. Introduction

The measurement of multiple cosmogenic nuclides [*Granger et al.*, 2013; *Lal*, 1988; *Nishiizumi et al.*, 1993; *von Blanckenburg and Willenbring*, 2014] constrains the history of rock surfaces and sediments that have experienced burial [*Granger*, 2006] or long-lived subaerial weathering [*Klein et al.*, 1986; *Nishiizumi et al.*, 1986]. Pairing two nuclides with different half-lives, such as ^{10}Be (~1.4 Ma) [*Chmeleff et al.*, 2010] and ^{26}Al (~0.7 Ma) [*Nishiizumi*, 2004], can detect complex sample histories involving the exposure/burial of surfaces covered by nonerosive glacial ice [*Bierman et al.*, 1999; *Stroeven et al.*, 2002], estimate the timing of sediment burial [*Balco and Rovey*, 2008; *Granger*, 2014; *Granger and Muzikar*, 2001], and quantify the exposure/erosion history of long-lived surfaces [*Brook et al.*, 1995]. Most two-nuclide cosmogenic isotope studies compare the measured $^{26}Al/^{10}Be$ ratio in quartz-bearing sample material to a nominal $^{26}Al/^{10}Be$ ratio at production [*Nishiizumi et al.*, 1991]; a sample $^{26}Al/^{10}Be$ ratio below that of the production ratio indicates burial or prolonged exposure.

The value of the $^{26}Al/^{10}Be$ production ratio remains uncertain for several reasons. (1) ^{26}Al has been measured much less frequently than ^{10}Be at production rate calibration sites. (2) Standards used to normalize measured isotopic ratios, as well as the assumed half-life of ^{10}Be, have changed over time [*Nishiizumi et al.*, 2007], but the assumed values of these parameters were typically not reported in most early publications estimating the $^{26}Al/^{10}Be$ production ratio (supporting information Table S1). (3) Although both ^{26}Al and ^{10}Be are produced predominately by neutron-induced spallation, muon interactions also produce these nuclides with an apparently higher $^{26}Al/^{10}Be$ production ratio [*Heisinger et al.*, 2002]. Hence, the measured $^{26}Al/^{10}Be$ of a sample is a combination of spallogenic nuclides and muogenic nuclides from the current period of exposure, as well as inherited spallogenic and muogenic nuclides from previous periods of exposure. (4) There are substantial challenges and uncertainties in estimating nuclide production ratios including accurate characterization of production cross sections at relevant neutron energies [*Caffee et al.*, 2013]. Together, these factors have prevented the accurate determination of the $^{26}Al/^{10}Be$ surface production ratio and its variation over latitude and altitude.

Because the $^{26}Al/^{10}Be$ production ratio is a key parameter in two-isotope interpretive models, the possibility that this ratio depends on geographic factors limits the accuracy of the two-isotope approach. This is especially relevant in the Arctic, where many $^{26}Al/^{10}Be$ ratios have been measured and interpreted to elucidate the exposure history of previously glaciated outcrops. The two-isotope approach has been used in Greenland [*Beel et al.*, 2016; *Corbett et al.*, 2016c, 2013; *Håkansson et al.*, 2009; *Roberts et al.*, 2008, 2009], Baffin Island [*Bierman et al.*, 2001; *Bierman et al.*, 1999; *Briner et al.*, 2006, 2003; *Corbett et al.*, 2016a; *Kaplan*

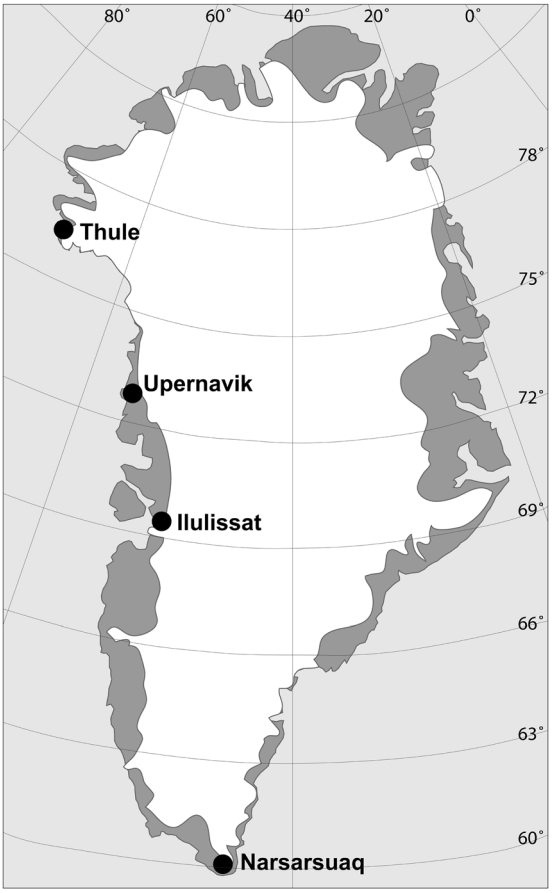

Figure 1. Map of Greenland showing the locations of the four study sites.

et al., 2001; *Margreth et al*., 2016; *Miller et al*., 2006], mainland Arctic Canada [*Marquette et al*., 2004], and Scandinavia [*Harbor et al*., 2006; *Stroeven et al*., 2002] to constrain the complex history of surfaces preserved beneath nonerosive glacial ice.

Here we measure the $^{26}Al/^{10}Be$ production ratio at high latitude (~61–77°N) in 24 samples collected from continuously exposed bedrock and boulder surfaces at four sites in Greenland (Figure 1). All of these sites were exposed during ice margin retreat at the end of the Last Glacial Maximum [*Bennike and Björck*, 2002; *Sinclair et al*., 2016]. The goal of this work is to use a field- and laboratory-based approach to further constrain the $^{26}Al/^{10}Be$ ratio at high latitude.

2. Previous Constraints on the $^{26}Al/^{10}Be$ Surface Production Ratio

Several different approaches have been used to estimate the $^{26}Al/^{10}Be$ production ratio, including direct measurement in young samples, inferences from long-exposed samples assumed to be at a secular equilibrium between production and decay, and model calculations (supporting information Table S1). Here, we report the original findings from these studies, without correcting for changes in nominal standard values and the ^{10}Be half-life; in Table S1, we scaled the inferred $^{26}Al/^{10}Be$ production ratios to currently accepted values.

Based on empirical analysis of field samples (representing nuclides produced from both spallation and muons), *Klein et al*. [1986] inferred a production ratio of ~7 in Libyan desert glass (25°N); *Nishiizumi et al*. [1989] obtained an average of 6.02 ± 0.44 (1σ) from quartz extracted from glacially polished Sierra Nevada granite (38°N); *Nishiizumi et al*. [1991] calculated ~6.2 from Antarctic bedrock (72°S), while *Brown et al*. [1991] calculated 6.5 ± 1.3 (1σ) from Antarctic moraines (78°S); *Larsen* [1996] measured 5.88 ± 1.02 (average, 1σ) in Laurentide Ice Sheet terminal moraine material (41°N); *Kubik et al*. [1998] determined a ratio of 6.52 ± 0.43 (weighted mean, 1σ) in Austrian landslide deposits (47°N); and *Nishiizumi et al*. [2005] calculated ~6.1 from alluvial fan deposits in Chile (27°S). Modeling and experimental studies estimated the spallation production ratio to be 6.11 [*Lal*, 1991], 7.1 [*Reedy et al*., 1994], and 6.05 [*Masarik and Reedy*, 1995].

Although there is spread in the measured production ratios and no systematic spatial trend, most of the original findings described above were consistent with a surface $^{26}Al/^{10}Be$ production ratio of ~6.1, and *Lal* [1991] adopted this ratio. It was used extensively in cosmogenic isotope studies until a change in the assumed value of primary accelerator standards [*Nishiizumi et al*., 2007], as well as updates to the ^{10}Be half-life [*Chmeleff et al*., 2010], raised the canonical $^{26}Al/^{10}Be$ surface spallation production ratio to ~6.75, which is the value that is currently used in the CRONUS Earth online calculator [*Balco et al*., 2008]. Recently, studies have refined cosmogenic nuclide production rates for different latitudes and altitudes. However, most measured only ^{10}Be, inferring ^{26}Al indirectly by use of the accepted spallogenic surface production ratio of 6.75 [*Balco et al*., 2009; *Briner et al*., 2012; *Goehring et al*., 2012; *Kaplan et al*., 2011; *Kelly et al*., 2015; *Putnam*

et al., 2010; *Young et al*., 2013a]. As such, these recent studies do not provide additional constraint of the $^{26}Al/^{10}Be$ production ratio.

A spallogenic $^{26}Al/^{10}Be$ production ratio exceeding 6.75 is consistent with modeling studies that investigated the latitude and/or altitude scaling of ^{10}Be and ^{26}Al independently [*Argento et al*., 2013; *Lifton et al*., 2014]. *Argento et al*. [2013], focusing on the high latitudes, modeled a spallogenic $^{26}Al/^{10}Be$ production ratio of ~7.0–7.1 for sea level (their Table 2) and found a small decrease in production ratio with increasing altitude (their Figure 6). A recent nuclide-specific scaling model [*Lifton et al*., 2014], based on analytical approximations of physics-based atmospheric cosmic ray fluxes similar to those used by *Argento et al*. [2013, 2015a, 2015b], found variation in the production ratio over both latitude and altitude (their Figure 8).

Using a more complete and refined representation of the physics involved, *Argento et al*. [2015a] also concluded that the $^{26}Al/^{10}Be$ production ratio varies with atmospheric depth (their Figure 6) but inferred a spallogenic surface production ratio of 6.7 at sea level and high latitude and lower ratios with increasing altitude. Because of the modeling refinements, they consider the 2015 results to supersede those from 2013. But while *Argento et al*. [2015a] cite improvements in radiation transport model physics in preferring the new results compared to those from 2013, they also note that they may be overestimating the ^{10}Be production rate by about 10% based on comparison with recent ^{10}Be calibration site data [*Phillips et al*., 2016], making their quoted $^{26}Al/^{10}Be$ production ratios underestimates. Given the different ^{26}Al and ^{10}Be excitation functions and the spallogenic nucleon energy spectra for the atmospheric depths relevant for in situ cosmogenic nuclide production, both *Argento et al*. [2015a] and *Lifton et al*. [2014] suggested that nuclide-specific scaling for altitude and latitude is appropriate. The new CRONUScalc online calculator [*Marrero et al*., 2016; *Phillips et al*., 2016] treats the two nuclides independently in terms of production rate models and thus production ratios.

Accompanying the numerical models, samples from calibration sites associated with the CRONUS-Earth project provide empirical constraint for the $^{26}Al/^{10}Be$ production ratio [*Phillips et al*., 2016]. Analytical results from CRONUS-Earth calibration samples presented in *Argento et al*. [2013] suggest that the $^{26}Al/^{10}Be$ production ratio (including both spallogenic and muogenic contributions) exceeds the canonical value of 6.75. Their Figure 7 shows that low-altitude (<2000 m) samples from six different calibration sites have a mean and median $^{26}Al/^{10}Be$ ratio of 7.2 ($1\sigma = 0.4$, interquartile range = 0.4, $n = 25$). Using data from selected CRONUS-Earth production rate calibration sites, *Borchers et al*. [2016] document surface $^{26}Al/^{10}Be$ ratios for Promontory Point, Utah (1598–1606 m above sea level (asl), 41°N: mean = 6.5, median = 6.6, $1\sigma = 0.7$, interquartile range = 0.8, $n = 19$), and Scotland (131–528 m asl, 57°N: mean = 7.3, median = 7.2, $1\sigma = 0.6$, interquartile range = 0.4, $n = 18$), suggesting that latitude and altitude may play important roles in surface production ratio scaling. However, the latitude and altitude of the calibration sites are internally correlated, as CRONUS-Earth sample sites tended to follow the snowline, leading to higher-altitude calibration sites at low-latitude and lower altitude calibration sites at high latitude.

3. Study Design and Assumptions

To assess the $^{26}Al/^{10}Be$ production ratio at high latitude, we present isotopic ratio data from four sites in Greenland spanning ~61–77°N and 50–724 m asl (Table 1 and Figure 1). Modeled production rates, scaled for latitude and altitude with both the CRONUS Earth online calculator [*Balco et al*., 2008] and the CRONUScalc online calculator [*Marrero et al*., 2016], are shown in supporting information Table S2 for each sample site. According to the CRONUS Earth online calculator [*Balco et al*., 2008], muon production represents $3.5 \pm 0.5\%$ of total ^{10}Be production and $4.3 \pm 0.6\%$ of total ^{26}Al production (average, 1 SD). According to the CRONUScalc online calculator [*Marrero et al*., 2016], muon production represents $1.4 \pm 0.2\%$ of total ^{10}Be production and $1.9 \pm 0.2\%$ of total ^{26}Al production (average, 1 SD). Since the CRONUS Earth online calculator [*Balco et al*., 2008] assumes a global $^{26}Al/^{10}Be$ spallation production ratio of 6.75, the summed spallogenic/muogenic $^{26}Al/^{10}Be$ production ratios for our samples are 6.79–6.82 (Table S2). Conversely, location-scaled production rates from the CRONUScalc online calculator [*Marrero et al*., 2016] yield summed spallogenic/muogenic $^{26}Al/^{10}Be$ production ratios of 7.26–7.30 (Tables 1 and S2).

The two southern study sites (Narsarsuaq, ~61°N [*Nelson et al*., 2014] and Ilulissat, ~69°N [*Corbett et al*., 2011]) were investigated previously using only ^{10}Be. The depth of glacial erosion has not been definitively

AGU Geophysical Research Letters

10.1002/2016GL071276

Table 1. Location and Isotopic Information for 24 Bedrock and Boulder Samples From Four Study Sites in Greenland[a]

Sample Name	Study Site[b]	Sample Type	Latitude (°N)	Longitude (°E)	Elevation (m asl)	^{10}Be Concentration ($\times10^4$ atoms g^{-1})	^{10}Be Uncertainty ($\times10^4$ atoms g^{-1})	^{26}Al Concentration ($\times10^5$ atoms g^{-1})	^{26}Al Uncertainty ($\times10^5$ atoms g^{-1})	^{26}Al/^{10}Be Ratio	^{26}Al/^{10}Be Uncertainty	Predicted ^{26}Al/^{10}Be Ratio[c]
GT022	Thule	Boulder	76.55833	−68.19445	358	6.455	0.199	4.386	0.175	6.79	0.34	7.28
GT023	Thule	Boulder	76.56945	−68.24887	346	6.304	0.215	4.707	0.194	7.47	0.40	7.28
GT055	Thule	Boulder	76.56046	−68.54910	201	5.488	0.205	4.092	0.174	7.46	0.42	7.30
GU002	Upernavik	Boulder	72.53587	−53.73338	603	8.059	0.191	5.588	0.431	6.93	0.56	7.26
GU104	Upernavik	Bedrock	72.77333	−55.50288	253	6.025	0.117	4.314	0.551	7.16	0.92	7.29
GL003	Ilulissat	Bedrock	69.43373	−50.26645	395	4.734	0.120	3.342	0.222	7.06	0.50	7.28
GL004	Ilulissat	Boulder	69.43379	−50.26637	392	4.993	0.119	3.515	0.138	7.04	0.32	7.28
GL080	Ilulissat	Bedrock	69.39508	−50.41634	621	6.183	0.138	4.493	0.152	7.27	0.30	7.26
GL081	Ilulissat	Boulder	69.39530	−50.41563	618	6.010	0.113	4.858	0.227	8.08	0.41	7.26
GL088	Ilulissat	Bedrock	69.34380	−50.42943	95	3.493	0.105	2.942	0.137	8.42	0.47	7.30
GL089	Ilulissat	Boulder	69.34380	−50.42911	93	3.612	0.081	2.557	0.170	7.08	0.50	7.30
GL105	Ilulissat	Bedrock	69.29280	−50.60203	300	4.655	0.108	3.210	0.163	6.90	0.38	7.29
GL106	Ilulissat	Boulder	69.29280	−50.60203	300	4.576	0.094	3.339	0.129	7.30	0.32	7.29
GL107	Ilulissat	Bedrock	69.17960	−50.89068	53	3.663	0.081	2.676	0.147	7.30	0.43	7.30
GL108	Ilulissat	Boulder	69.17960	−50.89068	53	3.730	0.103	2.594	0.162	6.96	0.47	7.30
GLX14B	Narsarsuaq	Bedrock	61.29564	−45.57079	307	5.963	0.116	4.191	0.176	7.03	0.33	7.29
GLX16A	Narsarsuaq	Boulder	61.32355	−45.53717	467	6.964	0.137	5.417	0.202	7.78	0.33	7.27
GLX16B	Narsarsuaq	Bedrock	61.32281	−45.53704	469	7.267	0.141	5.361	0.160	7.38	0.26	7.27
GLX17A	Narsarsuaq	Boulder	61.33134	−45.54345	724	9.108	0.247	6.431	0.197	7.06	0.29	7.25
GLX17B	Narsarsuaq	Bedrock	61.33136	−45.54328	720	8.004	0.561	6.432	0.272	8.04	0.66	7.25
GLX25A[d]	Narsarsuaq	Boulder	61.19340	−45.30210	556	8.171	0.199	4.962	0.165	6.07	0.25	7.27
GLX25B	Narsarsuaq	Bedrock	61.19338	−45.30169	554	7.787	0.152	5.841	0.192	7.50	0.29	7.27
GLX28A	Narsarsuaq	Boulder	60.99539	−45.43148	52	4.709	0.196	3.931	0.253	8.35	0.64	7.30
GLX28B	Narsarsuaq	Bedrock	60.99537	−45.43146	50	4.667	0.119	3.681	0.172	7.89	0.42	7.30

[a]Uncertainties are 1σ. Information about AMS measurement standards, isotopic ratios, sample masses, and ICP-quantified total Al is reported in supporting information Table S3 for all samples. Details about the preparation and measurement of the 24 ^{10}Be analyses and the five previously published ^{26}Al analyses, including ratios and blank corrections, are reported in the original publications containing the data. Information about background values for the new Al analyses is shown in Tables S4 and S5 .

[b]Previously published data: Thule, Al and Be, *Corbett et al.* [2016c, 2015]; Upernavik, Al and Be, *Corbett et al.* [2013]; Ilulissat, Be only, *Corbett et al.* [2011]; and Narsarsuaq, Be only, *Nelson et al.* [2014].

[c]Predicted production ratios were calculated for each sample site using the CRONUScalc online calculator [*Marrero et al.*, 2016] and SA scaling [*Lifton et al.*, 2014].

[d]We treat this sample as an outlier (see text for details) and exclude it from our data analysis.

determined, but the existence of streamlined and striated bedrock, as well as many ^{10}Be exposure ages coincident with local radiocarbon chronologies (especially in Ilulissat), argues that the depth of erosion was at least several meters, removing all spallogenic nuclides from prior periods of exposure [*Corbett et al*., 2011; *Cronauer et al*., 2016; *Kelley et al*., 2013; *Nelson et al*., 2014; *Young et al*., 2013b; *Young et al*., 2011]. For these two sites, the Al sample fraction was archived after initial sample preparation; we recovered and analyzed that archived material (19 samples in total) for this study.

The two northern study sites (Upernavik, ~73°N [*Corbett et al*., 2013] and Thule, ~77°N [*Corbett et al*., 2015, 2016c]) were previously investigated with paired ^{26}Al and ^{10}Be, and we make use of a subset of those data. Upernavik is characterized by deeply eroded fjords separated by highlands preserved beneath nonerosive glacial ice; here, we include only samples from low elevations in the fjords [*Corbett et al*., 2013]. Thule experienced heterogeneous subglacial erosion, and its boulders contain varying amounts of nuclides inherited from previous periods of exposure; here, we utilize only the boulders that have ^{10}Be exposure ages coincident with radiocarbon estimates of deglaciation timing [*Corbett et al*., 2015].

Although we are unable to determine the depth of erosion during the last glaciation, we infer that it was at least several meters because inherited nuclide concentrations from previous periods of exposure are demonstrably low in the sample surfaces included here. If any of the samples do contain spallogenic nuclides from previous periods of exposure, the shorter half-life of ^{26}Al would drive the ^{26}Al/^{10}Be ratio downward during times of burial. Therefore, the ^{26}Al/^{10}Be production ratios we infer would represent underestimates.

We do not think it is likely that muogenic production has made an appreciable impact on our inferred ^{26}Al/^{10}Be production ratio. Penetrating more deeply into Earth's surface, muons [*Heisinger et al*., 2002] produce ^{10}Be and ^{26}Al at rates that are only a few percent of spallation production rates (Table S2). The ^{26}Al/^{10}Be muon production ratio is not well constrained, but a value of ~8.35 is used in the CRONUS Earth online calculator [*Balco et al*., 2008] and ~9.75 in the CRONUScalc online calculator [*Marrero et al*., 2016] for the locations of our sample sites (Table S2). Although the muogenic ^{26}Al/^{10}Be production ratio is higher than that of spallation, nuclides produced by muons during the present interglacial period represent such a small fraction of total isotope production that their impact on the surface production ratio is minimal.

Inherited nuclides from muogenic production are also unlikely to be important. Muogenic nuclides from previous periods of exposure may exist in sample surfaces independent of subglacial erosion history because muons penetrate deeply; thus, even efficient glacial erosion is incapable of stripping away all muon-produced nuclides [*Briner et al*., 2016]. However, nuclides inherited from previous interglacial periods when our sample sites were ice free would have experienced burial following initial exposure, lowering the ^{26}Al/^{10}Be ratio by radioactive decay.

4. Methods

All samples were prepared at the University of Vermont using standard procedures [*Corbett et al*., 2016b]. Additions of ^{27}Al carrier (1000 μg mL^{-1} SPEX Al standard) were optimized to reach a total of ~1500–2500 μg Al in each sample based on quantification of native Al in purified quartz. We quantified total ^{27}Al in the samples immediately following digestion with inductively coupled plasma optical emission spectrometry (ICP-OES) analysis of replicate aliquots using two emission lines (308.215 and 309.271 nm) and an internal standard (Ga).

We recovered archived Al sample fractions from Narsarsuaq ($n = 9$) and Ilulissat ($n = 10$) in 2016 (Table 1); these samples, which were stored as Al hydroxide gels since 2011 (Ilulissat) and 2014 (Narsarsuaq), had dried fully despite being in capped centrifuge tubes. We reconstituted the pellets in heated 10% nitric acid and reprecipitated Al hydroxide at pH 8. To remove Mg, which forms an isobar that interferes with ^{26}Al analysis on the Purdue Rare Isotope Measurement (PRIME) Laboratory Accelerator Mass Spectrometer (AMS), we used a modified cation chromatography method. Our standard Be elution (five column volumes of 1.2 N HCl [*Corbett et al*., 2016b]) was followed by a Mg elution (an additional eight column volumes of 1.2 N HCl) before elution of Al (four column volumes of 4 N HCl). ICP-OES analysis of small aliquots from the samples after processing indicated that sample recovery was 75 ± 11% (average, 1σ, $n = 19$) of the original total Al in the samples.

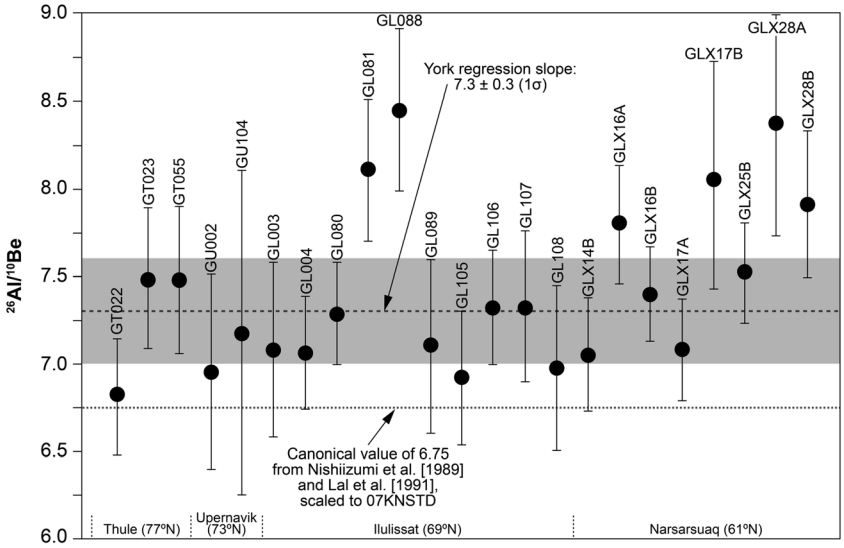

Figure 2. Calculated ^{26}Al/^{10}Be ratios for each of the 23 bedrock and boulder samples (excluding one outlier). Error bars show ±1σ, with errors from the two individual isotopes propagated in quadrature. Samples are sorted by site along the *x* axis.

Isotope ratios (supporting information Table S3) reported in the original publications [*Corbett et al*., 2016c; *Corbett et al*., 2015, 2013, 2011; *Nelson et al*., 2014] were measured by AMS at Lawrence Livermore National Laboratory (^{10}Be/^{9}Be from Narsarsuaq, Ilulissat, and Upernavik, as well as ^{26}Al/^{27}Al from Upernavik) and Scottish Universities Environmental Research Centre (^{10}Be/^{9}Be and ^{26}Al/^{27}Al from Thule). Isotope ratios for the new ^{26}Al/^{27}Al data reported here were measured at PRIME Laboratory. For the new ^{26}Al/^{27}Al analyses from Narsarsuaq and Ilulissat (supporting information Table S3), ICP-quantified total Al ranged from 1433 to 3115 μg. Sample ratios were normalized to standard KNSTD with an assumed ratio of 1.818×10^{-12} [*Nishiizumi*, 2004]. Measured ratios for the new ^{26}Al analyses ($n = 19$) ranged from 6.2 to 41.2×10^{-14}, and analytic uncertainties were 4.8 ± 1.4% (average, 1σ).

Measured ^{26}Al/^{27}Al ratios for process blanks ($n = 6$; supporting information Table S4 and Figure S1) at PRIME Laboratory were scattered, with four blanks yielding low, indistinguishable ratios averaging 7.7×10^{-16} and the remaining two blanks almost an order of magnitude higher with ratios of 6.1×10^{-15} (from the Ilulissat study) and 7.5×10^{-15} (from the Narsarsuaq study). We chose to discard the high ^{26}Al blank from the Narsarsuaq study since it was discarded in the original publication of the ^{10}Be data, where it was the only elevated blank of nine that were measured [*Nelson et al*., 2014].

To account for multiple possible blank corrections for the new ^{26}Al PRIME Laboratory measurements, we performed a sensitivity analysis utilizing four different backgrounds (supporting information Table S5): mean or median blank value with the high Ilulissat blank included or excluded. All four possibilities use one standard deviation around the mean to propagate blank uncertainty into the sample uncertainties in quadrature. The sensitivity analysis demonstrates that the difference between blank corrections is small; calculated ^{26}Al/^{10}Be ratios vary by only 0.06 ± 0.04 across all four scenarios, resulting in a 0.8 ± 0.5% difference ($n = 19$, average, 1σ). For the new ^{26}Al analyses presented in this manuscript, we chose to use the median blank value (without discarding the high Ilulissat blank) and one standard deviation around the mean, which yields a ^{26}Al/^{27}Al background of $6.9 \pm 24.6 \times 10^{-16}$. We subtracted the blank ratio from all samples and propagated uncertainties in quadrature; this blank represents a 0.2–1.1% (average 0.4 ± 0.2%, 1σ) correction of the sample ratios. The ^{26}Al concentrations and ^{26}Al/^{10}Be ratios for the four possible blank corrections are shown in the supporting information (Table S5).

5. Results

Our measurements of stable ^{27}Al, an important aspect of quantifying ^{26}Al, are robust. For the blanks included in the 10 batches of samples described here, the expected (as determined through the addition of ^{27}Al carrier)

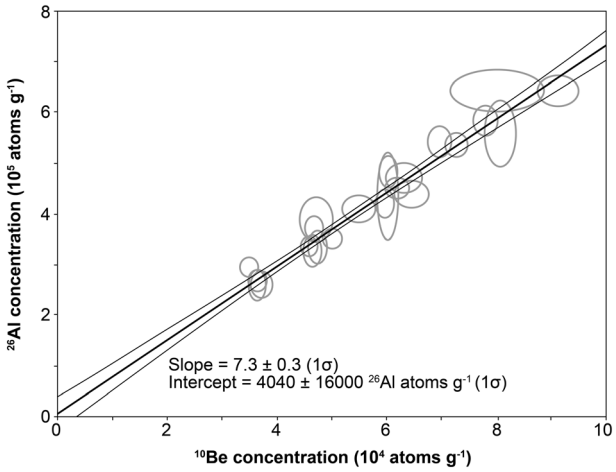

Figure 3. York regression of ^{26}Al concentrations versus ^{10}Be concentrations ($n = 23$, excluding one outlier). Gray ellipses show samples' 1σ error for each of the two isotopes. Heavy dark line shows the uncertainty-weighted trendline through the data set; thin dark lines show the 1σ uncertainty envelope around the trendline.

and the measured (as determined through ICP-OES analysis) Al contents differ by only $2.0 \pm 2.4\%$ (absolute value, $n = 13$, 1σ). This indicates that ICP-OES quantification of total Al in samples is accurate, with little or no loss of Al through precipitation of fluoride compounds [*Bierman and Caffee*, 2002]. The long-term calculated ^{26}Al concentration of the quality control material CRONUS-N in the University of Vermont Laboratory is $1.03 \pm 0.06 \times 10^6$ atoms g^{-1} (average, $n = 20$, 1σ), which is indistinguishable from the value of $1.05 \pm 0.11 \times 10^6$ atoms g^{-1} ($n = 10$, 1σ) obtained by *Jull et al.* [2015].

Across the data set as a whole, blank-corrected sample ^{10}Be concentrations range from 3.5 to 9.1×10^4 atoms g^{-1} and ^{26}Al concentrations range from 2.6 to 6.4×10^5 atoms g^{-1} ($n = 24$, Table 1). Calculated ^{26}Al/^{10}Be ratios are 6.07–8.42, with uncertainties of $5.8 \pm 2.0\%$ ($n = 24$, average, 1σ; Table 1). However, the lowest calculated ^{26}Al/^{10}Be ratio (GLX25A, 6.07 ± 0.25) is $>2\sigma$ below the data set mean and is a statistical outlier using Peirce's criterion; we therefore infer that this sample likely records a complex history and omit it from our further calculations.

After omission of sample GLX25A, the calculated ^{26}Al/^{10}Be ratios range from 6.79 to 8.42 ($n = 23$, Table 1 and Figure 2). The arithmetic mean ^{26}Al/^{10}Be ratio for the entire data set is 7.4 ± 0.5 ($n = 23$, 1σ). The median, similar to the mean, is 7.3, and the interquartile range is 0.6. The direct uncertainty-weighted mean is 7.3 ± 0.1 (1σ). A York regression, which accounts for uncertainties in both ^{10}Be and ^{26}Al, gives a slope (i.e., ^{26}Al/^{10}Be ratio) of 7.3 ± 0.3 (1σ) and a y intercept that is statistically indistinguishable from zero at 1σ (Figure 3). There is no statistically significant spatial variability of ^{26}Al/^{10}Be ratio within the limited latitude/altitude range of the study area, consistent with theoretical predictions [*Argento et al.*, 2013; *Argento et al.*, 2015b; *Lifton et al.*, 2014]; sample ^{26}Al/^{10}Be ratios are not significantly correlated with latitude ($R^2 = 0.03$, $p = 0.39$) or altitude ($R^2 = 0.03$, $p = 0.41$), nor are they separable by site ($p = 0.80$ using a one-way analysis of variance).

6. Discussion

Analysis of paired ^{26}Al/^{10}Be data from continuously exposed samples in Greenland indicates that the high-latitude, low-altitude ^{26}Al/^{10}Be surface production ratio in quartz, incorporating both spallation and muon interactions, is 7.3 ± 0.3 (slope of a York regression, 1σ, Figure 3). Assuming a muon contribution of 1.5%, a muogenic ^{26}Al/^{10}Be production ratio of 9.75 [*Marrero et al.*, 2016], and a summed spallogenic/muogenic ^{26}Al/^{10}Be production ratio of 7.3, we calculate a spallation-only ^{26}Al/^{10}Be production ratio of 7.25. This value is about 8% higher than the currently accepted spallation value of 6.75 ± 0.5 (based on *Nishiizumi et al.* [1986], normalized to standard values presented in *Nishiizumi et al.* [2007]).

It seems unlikely that analytic uncertainties alone explain the differences in the measured production ratios; rather, we suggest that latitude dependence or other site-specific factors control the production ratio. A production ratio exceeding 6.75 is consistent with other studies that investigated the scaling of ^{10}Be and ^{26}Al independently, especially the values presented in *Argento et al.* [2013] and *Lifton et al.* [2014]. The production ratio we calculate here exceeds the value of ~6.7 that *Argento et al.* [2015b] inferred for sea level and high latitude, which is more consistent with the canonical value. However, the findings of *Argento et al.* [2015b] may be biased by a ^{10}Be production rate that is ~10% too high; correcting the ^{10}Be production rate

downward, their inferred $^{26}Al/^{10}Be$ production ratio is ~7.4, which aligns closely with the value we determined in Greenland. The production ratio we measure here agrees with site-specific production ratios (Tables 1 and S2) calculated using the CRONUScalc online calculator [*Marrero et al*., 2016] and "SA" scaling [*Lifton et al*., 2014].

Available published data are not sufficient to fully evaluate the scaling of the $^{26}Al/^{10}Be$ production ratio over space due to two key limitations. First, in the past, ^{26}Al measurements typically had greater statistical uncertainties than ^{10}Be measurements, yielding low-precision $^{26}Al/^{10}Be$ ratios. Second, no systematic studies with high-precision measurements have been conducted in which the production ratios were measured in a suite of samples where only one geographic parameter (latitude, for example) varied. Such studies are needed to clarify the $^{26}Al/^{10}Be$ production ratio at different latitudes and altitudes.

The $^{26}Al/^{10}Be$ surface production ratio in quartz has important implications for the histories inferred using cosmogenic nuclide analysis in bedrock and boulder surfaces. A higher than currently accepted $^{26}Al/^{10}Be$ production ratio would result in more samples that record a history of burial and longer modeled burial durations. As demonstrated by a sensitivity analysis in *Corbett et al*. [2016c], an assumed $^{26}Al/^{10}Be$ production ratio of 7.35 results in the conclusion that 61% of boulders in the data set experienced burial, whereas an assumed production ratio of 6.75 suggests that only 21% of boulders have been buried (where burial is defined by a sample point falling $>1\sigma$ below the constant production or steady erosion curve). Further, for every 0.1 increase in assumed production ratio, modeled burial durations for a representative sample in *Corbett et al*. [2016c] increased by 53 kyr. Thus, the change we suggest here (from 6.75 to 7.3) would increase the burial age for that sample by nearly 300 kyr.

7. Conclusions

Analysis of continuously exposed quartz-bearing bedrock and boulder surfaces spanning ~61–77°N in Greenland yields a surface $^{26}Al/^{10}Be$ production ratio of 7.3 ± 0.3 (slope of a York regression, 1σ, spallogenic and muogenic production). The surfaces we analyzed here were eroded during the last glaciation, appear to have simple exposure histories (excluding one outlier), and have been exposed since ice retreated across the landscape at the beginning of the Holocene. The $^{26}Al/^{10}Be$ ratio we determine is ~8% greater than that used for most studies, suggesting that the canonical production ratio is not appropriate for at least certain areas of the world, likely because production rates of these two cosmogenic nuclides do not scale similarly over space. Since most two-isotope cosmogenic studies rely on the $^{26}Al/^{10}Be$ surface production ratio as a central assumption, this new constraint on the ratio has important implications for inferred exposure, burial, and erosion histories, especially in the Arctic. Our results suggest that additional production ratio calibrations are necessary globally.

Acknowledgments
Funding was provided by National Science Foundation (NSF) ARC-0713956 and NSF ARC-1023191 to Bierman and NSF BCS-1433878 to Corbett. Corbett was also supported by an NSF Graduate Research Fellowship and grants from Geological Society of America Quaternary Geology and Geomorphology Division J. Hoover Mackin Award and the International Association of Geochemistry. We thank CH2MHILL Polar Services for support during fieldwork. Caffee and Woodruff acknowledge support from NSF EAR-0919759; Lifton acknowledges support from NSF EAR-1560658. D. Argento and one anonymous reviewer provided suggestions that improved the manuscript. Data from this study are available in Table 1 as well as in Tables S1–S5 of the supporting information.

References

Argento, D., R. Reedy, and J. Stone (2013), Modeling the Earth's cosmic radiation, *Nucl. Instrum. Meth. Phys. Res. B*, *294*, 464–469.
Argento, D., J. Stone, R. Reedy, and K. O'Brien (2015a), Physics-based modeling of cosmogenic nuclides part I—Radiation transport methods and new insights, *Quat. Geochronol.*, *26*, 29–43.
Argento, D., J. Stone, R. Reedy, and K. O'Brien (2015b), Physics-based modeling of cosmogenic nuclides part II—Key aspects of in-situ cosmogenic nuclide production, *Quat. Geochronol.*, *26*, 44–55.
Balco, G., and C. Rovey (2008), An isochron method for cosmogenic-nuclide dating of buried soils and sediments, *Am. J. Sci.*, *308*, 1083–1114.
Balco, G., J. Stone, N. Lifton, and T. Dunai (2008), A complete and easily accessible means of calculating surface exposure ages or erosion rates from ^{10}Be and ^{26}Al measurements, *Quat. Geochronol.*, *3*(3), 174–195.
Balco, G., J. Briner, R. Finkel, J. Rayburn, J. Ridge, and J. Schaefer (2009), Regional beryllium-10 production rate calibration for late-glacial northeastern North America, *Quat. Geochronol.*, *4*(2), 93–107.
Beel, C., N. Lifton, J. Briner, and B. Goehring (2016), Quaternary evolution and ice sheet history of contrasting landscapes in Uummannaq and Sukkertoppen, western Greenland, *Quat. Sci. Rev.*, *149*, 248–258.
Bennike, O., and S. Björck (2002), Chronology of the last recession of the Greenland ice sheet, *J. Quat. Sci.*, *17*(3), 211–219.
Bierman, P., and M. Caffee (2002), Cosmogenic exposure and erosion history of Australian bedrock landforms, *Bull. Geol. Soc. Am.*, *114*(7), 787–803.
Bierman, P., K. Marsella, C. Patterson, P. Davis, and M. Caffee (1999), Mid-Pleistocene cosmogenic minimum-age limits for pre-Wisconsinan glacial surfaces in southwestern Minnesota and southern Baffin Island: A multiple nuclide approach, *Geomorphology*, *27*(1), 25–39.
Bierman, P., K. Marsella, P. Davis, and M. Caffee (2001), Response to discussion by Wolfe et al. on Bierman et al. (Geomorphology 25 (1999) 25–39), *Geomorphology*, *39*, 255–260.
Borchers, B., S. Marrero, G. Balco, M. Caffee, B. Goehring, N. Lifton, K. Nishiizumi, F. Phillips, J. Schaefer, and J. Stone (2016), Geological calibration of spallation production rates in the CRONUS-Earth project, *Quat. Geochronol.*, *31*, 188–198.

Briner, J., G. Miller, P. Davis, P. Bierman, and M. Caffee (2003), Last Glacial Maximum ice sheet dynamics in Arctic Canada inferred from young erratics perched on ancient tors, *Quat. Sci. Rev.*, *22*(5–7), 437–444.
Briner, J., G. Miller, P. Davis, and R. Finkel (2006), Cosmogenic radionuclides from fjord landscapes support differential erosion by overriding ice sheets, *Geol. Soc. Am. Bull.*, *118*(3/4), 406–420.
Briner, J., N. Young, B. Goehring, and J. Schaefer (2012), Constraining Holocene ^{10}Be production rates in Greenland, *J. Quat. Sci.*, *27*(1), 2–6.
Briner, J., B. Goehring, J. Mangerud, and J. Svendsen (2016), The deep accumulation of ^{10}Be at Utsira, southwestern Norway: Implications for cosmogenic nuclide exposure dating in peripheral ice sheet landscapes, *Geophys. Res. Lett.*, *43*, 9121–9129, doi:10.1002/2016GL070100.
Brook, E., E. Brown, M. Kurz, R. Ackert, G. Raisbeck, and F. Yiou (1995), Constraints on age, erosion, and uplift of Neogene glacial deposits in the Transantarctic Mountains determined from in situ cosmogenic ^{10}Be and ^{26}Al, *Geology*, *23*(12), 1063–1066.
Brown, E., J. Edmond, G. Raisbeck, F. Yiou, M. Kurz, and E. Brook (1991), Examination of surface exposure ages of Antarctic moraines using in situ produced ^{10}Be and ^{26}Al, *Geochim. Cosmochim. Acta*, *55*(8), 2269–2283.
Caffee, M., K. Nishiizumi, J. Sisterson, J. Ullmann, and K. Welten (2013), Cross section measurements at neutron energies 71 and 112 MeV and energy integrated cross section measurements ($0.1 < E_n < 750$ MeV) for the neutron induced reactions O(n, x)^{10}Be, Si(n, x)^{10}Be, and Si(n, x)^{26}Al, *Nucl. Instrum. Meth. Phys. Res. Sect. B: Beam Int. Mater. Atoms*, *294*, 479–483.
Chmeleff, J., F. Von Blanckenburg, K. Kossert, and D. Jakob (2010), Determination of the ^{10}Be half-life by multicollector ICP-MS and liquid scintillation counting, *Nucl. Instrum. Meth. Phys. Res. Sect. B: Beam Int. Mater. Atoms*, *268*(2), 192–199.
Corbett, L., N. Young, P. Bierman, J. Briner, T. Neumann, J. Graly, and D. Rood (2011), Paired bedrock and boulder ^{10}Be concentrations resulting from early Holocene ice retreat near Jakobshavn Isfjord, western Greenland, *Quat. Sci. Rev.*, *30*, 1739–1749.
Corbett, L., P. Bierman, J. Graly, T. Neumann, and D. Rood (2013), Constraining landscape history and glacial erosivity using paired cosmogenic nuclides in Upernavik, northwest Greenland, *Geol. Soc. Am. Bull.*, *125*(9/10), 1539–1553.
Corbett, L., P. Bierman, G. Lasher, and D. Rood (2015), Landscape chronology and glacial history in Thule, northwest Greenland, *Quat. Sci. Rev.*, *109*, 57–67.
Corbett, L., P. Bierman, and P. Davis (2016a), Glacial history and landscape evolution of southern Cumberland Peninsula, Baffin Island, Canada, constrained by cosmogenic ^{10}Be and ^{26}Al, *Geol. Soc. Am. Bull.*, *128*, 1173–1192.
Corbett, L., P. Bierman, and D. Rood (2016b), An approach for optimizing in situ cosmogenic ^{10}Be sample preparation, *Quat. Geochronol.*, *33*, 24–34.
Corbett, L., P. Bierman, and D. Rood (2016c), Constraining multi-stage exposure-burial scenarios for boulders preserved beneath cold-based glacial ice in Thule, northwest Greenland, *Earth Planet. Sci. Lett.*, *440*, 147–157.
Cronauer, S., J. Briner, S. Kellet, S. Zimmerman, and M. Morlighem (2016), ^{10}Be dating reveals early-middle Holocene age of the Drygalski moraines in central west Greenland, *Quat. Sci. Rev.*, *147*, 59–68.
Goehring, B., Ø. Lohne, J. Mangerud, J. Svendsen, R. Gyllencreutz, J. Schaefer, and R. Finkel (2012), Late glacial and Holocene ^{10}Be production rates for western Norway, *J. Quat. Sci.*, *27*(1), 89–96.
Granger, D. (2006), A review of burial dating methods using ^{26}Al and ^{10}Be, *Geol. Soc. Am. Spec. Pap.*, *415*, 1–16.
Granger, D. (2014), Cosmogenic nuclide burial dating in archaeology and paleoanthropology, in *Treatise on Geochemistry*, 2nd ed., vol. 14, edited by H. Holland and K. Turekian, pp. 81–97, Elsevier, Oxford.
Granger, D., and P. Muzikar (2001), Dating sediment burial with in situ-produced cosmogenic nuclides: Theory, techniques, and limitations, *Earth Planet. Sci. Lett.*, *188*(1–2), 269–281.
Granger, D., N. Lifton, and J. Willenbring (2013), A cosmic trip: 25 years of cosmogenic nuclides in geology, *Geol. Soc. Am. Bull.*, *125*(9–10), 1379–1402.
Håkansson, L., H. Alexanderson, C. Hjort, P. Moller, J. Briner, A. Aldahan, and G. Possnert (2009), Late Pleistocene glacial history of Jameson Land, central East Greenland, derived from cosmogenic ^{10}Be and ^{26}Al exposure dating, *Boreas*, *38*(2), 244–260.
Harbor, J., A. Stroeven, D. Fabel, A. Clarhäll, J. Kleman, Y. Li, D. Elmore, and D. Fink (2006), Cosmogenic nuclide evidence for minimal erosion across two subglacial sliding boundaries of the late glacial Fennoscandian ice sheet, *Geomorphology*, *75*(1–2), 90–99.
Heisinger, B., D. Lal, A. Jull, P. Kubik, S. Ivy-Ochs, S. Neumaier, K. Knie, V. Lazarev, and E. Nolte (2002), Production of selected cosmogenic radionuclides by muons: 1. Fast muons, *Earth Planet. Sci. Lett.*, *200*(3–4), 345–355.
Jull, A., E. Scott, and P. Bierman (2015), The CRONUS-Earth inter-comparison for cosmogenic isotope analysis, *Quat. Geochronol.*, *26*, 3–10.
Kaplan, M., G. Miller, and E. Steig (2001), Low-gradient outlet glaciers (ice streams?) drained the Laurentide ice sheet, *Geology*, *29*(4), 343–346.
Kaplan, M., J. Strelin, J. Schaefer, G. Denton, R. Finkel, R. Schwartz, A. Putnam, M. Vandergoes, B. Goehring, and S. Travis (2011), In-situ cosmogenic ^{10}Be production rate at Lago Argentino, Patagonia: Implications for late-glacial climate chronology, *Earth Planet. Sci. Lett.*, *309*(1), 21–32.
Kelley, S., J. Briner, and N. Young (2013), Rapid ice retreat in Disko Bugt supported by ^{10}Be dating of the last recession of the western Greenland ice sheet, *Quat. Sci. Rev.*, *82*, 13–22.
Kelly, M., T. Lowell, P. Applegate, F. Phillips, J. Schaefer, C. Smith, H. Kim, K. Leonard, and A. Hudson (2015), A locally calibrated, late glacial ^{10}Be production rate from a low-latitude, high-altitude site in the Peruvian Andes, *Quat. Geochronol.*, *26*, 70–85.
Klein, J., R. Giegengack, R. Middleton, P. Sharma, J. Underwood, and R. Weeks (1986), Revealing histories of exposure using in situ produced ^{26}Al and ^{10}Be in Libyan desert glass, *Radiocarbon*, *28*(2A), 547–555.
Kubik, P., S. Ivy-Ochs, J. Masarik, M. Frank, and C. Schluchter (1998), ^{10}Be and ^{26}Al production rates deduced from an instantaneous event within the dendro-calibration curve, the landslide of Kofels, Otz Valley, Austria, *Earth Planet. Sci. Lett.*, *161*, 231–241.
Lal, D. (1988), In situ-produced cosmogenic isotopes in terrestrial rocks, *Annu. Rev. Earth Planet. Sci.*, *16*(1), 355–388.
Lal, D. (1991), Cosmic ray labeling of erosion surfaces: In situ nuclide production rates and erosion models, *Earth Planet. Sci. Lett.*, *104*(2–4), 424–439.
Larsen, P. (1996), In-situ production rates of cosmogenic ^{10}Be and ^{26}Al over the past 21,500 years determined from the terminal moraine of the Laurentide Ice Sheet, North-Central New Jersey, 142 pp, University of Vermont, Burlington, Vermont.
Lifton, N., T. Sato, and T. Dunai (2014), Scaling in situ cosmogenic nuclide production rates using analytical approximations to atmospheric cosmic-ray fluxes, *Earth Planet. Sci. Lett.*, *386*, 149–160.
Margreth, A., J. Gosse, and A. Dyke (2016), Quantification of subaerial and episodic subglacial erosion rates on high latitude upland plateaus: Cumberland Peninsula, Baffin Island, Arctic Canada, *Quat. Sci. Rev.*, *133*, 108–129.
Marquette, G., J. Gray, J. Gosse, F. Courchesne, L. Stockli, G. Macpherson, and R. Finkel (2004), Felsenmeer persistence under non-erosive ice in the Torngat and Kaumajet mountains, Quebec and Labrador, as determined by soil weathering and cosmogenic nuclide exposure dating, *Can. J. Earth Sci.*, *41*(1), 19–38.
Marrero, S., F. Phillips, B. Borchers, N. Lifton, R. Aumer, and G. Balco (2016), Cosmogenic nuclide systematics and the CRONUScalc program, *Quat. Geochronol.*, *31*, 160–187.

Masarik, J., and R. Reedy (1995), Terrestrial cosmogenic-nuclide production systematics calculated from numerical simulations, *Earth Planet. Sci. Lett.*, *136*(3), 381–395.

Miller, G., J. Briner, N. Lifton, and R. Finkel (2006), Limited ice-sheet erosion and complex exposure histories derived from in situ cosmogenic ^{10}Be, ^{26}Al, and ^{14}C on Baffin Island, Arctic Canada, *Quat. Geochronol.*, *1*, 74–85.

Nelson, A., P. Bierman, J. Shakun, and D. Rood (2014), Using in situ cosmogenic ^{10}Be to identify the source of sediment leaving Greenland, *Earth Surf. Processes Landforms*, *39*, 1087–1100.

Nishiizumi, K. (2004), Preparation of ^{26}Al AMS standards, *Nucl. Instrum. Meth. Phys. Res. Sect. B: Beam Int. Mater. Atoms*, *223–224*, 388–392.

Nishiizumi, K., D. Lal, J. Klein, R. Middleton, and J. Arnold (1986), Production of ^{10}Be and ^{26}Al by cosmic rays in terrestrial quartz in situ and implications for erosion rates, *Nature*, *319*, 134–136.

Nishiizumi, K., E. Winterer, C. Kohl, J. Klein, R. Middleton, D. Lal, and J. Arnold (1989), Cosmic ray production rates of ^{10}Be and ^{26}Al in quartz from glacially polished rocks, *J. Geophys. Res.*, *94*, 17,907–17,915, doi:10.1029/JB094iB12p17907.

Nishiizumi, K., C. Kohl, J. Arnold, J. Klein, D. Fink, and R. Middleton (1991), Cosmic ray produced ^{10}Be and ^{26}Al in Antarctic rocks: Exposure and erosion history, *Earth Planet. Sci. Lett.*, *104*(2–4), 440–454.

Nishiizumi, K., C. Kohl, J. Arnold, R. Dorn, I. Klein, D. Fink, R. Middleton, and D. Lal (1993), Role of in situ cosmogenic nuclides ^{10}Be and ^{26}Al in the study of diverse geomorphic processes, *Earth Surf. Processes Landforms*, *18*(5), 407–425.

Nishiizumi, K., M. Caffee, R. Finkel, G. Brimhall, and T. Mote (2005), Remnants of a fossil alluvial fan landscape of Miocene age in the Atacama Desert of northern Chile using cosmogenic nuclide exposure age dating, *Earth Planet. Sci. Lett.*, *237*(3), 499–507.

Nishiizumi, K., M. Imamura, M. Caffee, J. Southon, R. Finkel, and J. McAninch (2007), Absolute calibration of ^{10}Be AMS standards, *Nucl. Instrum. Meth. Phys. Res. Sect. B: Beam Int. Mater. Atoms*, *258*(2), 403–413.

Phillips, F., et al. (2016), The CRONUS-Earth project: A synthesis, *Quat. Geochronol.*, *31*, 119–154.

Putnam, A., J. Schaefer, D. Barrell, M. Vandergoes, G. Denton, M. Kaplan, R. Finkel, R. Schwartz, B. Goehring, and S. Kelley (2010), In situ cosmogenic ^{10}Be production-rate calibration from the Southern Alps, New Zealand, *Quat. Geochronol.*, *5*(4), 392–409.

Reedy, R., K. Nishiizumi, D. Lal, J. Arnold, P. Englert, J. Klein, R. Middleton, A. Jull, and D. Donahue (1994), Simulations of terrestrial in-situ cosmogenic nuclide production, *Nucl. Inst. Meth. Phys. Res. B*, *92*, 297–300.

Roberts, D., A. Long, C. Schnabel, S. Freeman, and M. Simpson (2008), The deglacial history of southeast sector of the Greenland ice sheet during the Last Glacial Maximum, *Quat. Sci. Rev.*, *27*, 1505–1516.

Roberts, D., A. Long, C. Schnabel, B. Davies, S. Xu, M. Simpson, and P. Huybrechts (2009), Ice sheet extent and early deglacial history of the southwestern sector of the Greenland ice sheet, *Quat. Sci. Rev.*, *28*, 2760–2773.

Sinclair, G., A. Carlson, A. Mix, B. Lecavalier, G. Milne, A. Mathias, C. Buizert, and R. DeConto (2016), Diachronous retreat of the Greenland ice sheet during the last deglaciation, *Quat. Sci. Rev.*, *145*, 243–258.

Stroeven, A., D. Fabel, C. Hattestrand, and J. Harbor (2002), A relict landscape in the centre of Fennoscandian glaciation: Cosmogenic radionuclide evidence of tors preserved through multiple glacial cycles, *Geomorphology*, *44*(1–2), 145–154.

von Blanckenburg, F., and J. Willenbring (2014), Cosmogenic nuclides: Dates and rates of Earth-surface change, *Elements*, *10*(5), 341–346.

Young, N., J. Briner, H. Stewart, Y. Axford, B. Csatho, D. Rood, and R. Finkel (2011), Response of Jakobshavn Isbrae, Greenland, to Holocene climate change, *Geology*, *39*(2), 131–134.

Young, N., J. Schaefer, J. Briner, and B. Goehring (2013a), A ^{10}Be production-rate calibration for the Arctic, *J. Quat. Sci.*, *28*(5), 515–526.

Young, N., J. Briner, D. Rood, R. Finkel, L. Corbett, and P. Bierman (2013b), Age of the Fjord Stade moraines in the Disko Bugt region, western Greenland, and the 9.3 and 8.2 ka cooling events, *Quat. Sci. Rev.*, *60*, 76–90.